JOURNAL OF CATALYSIS **165,** 162–171 (1997)
ARTICLE NO. CA971484

Lactic Acid Conversion to 2,3-Pentanedione and Acrylic Acid over Silica-Supported Sodium Nitrate: Reaction Optimization and Identification of Sodium Lactate as the Active Catalyst

Douglas C. Wadley,* Man S. Tam,* Prashant B. Kokitkar,† James E. Jackson,† and Dennis J. Miller*,[1]

Department of Chemical Engineering and †Department of Chemistry, Michigan State University, East Lansing, Michigan 48824

Received March 14, 1996; revised October 2, 1996; accepted October 7, 1996

Lactic acid is converted to 2,3-pentanedione, acrylic acid, and other products in vapor-phase reactions over silica-supported sodium lactate formed from sodium nitrate. Multiparameter optimization of reaction conditions using a Box–Benkhen experimental design shows that the highest yield and selectivity to 2,3-pentanedione are achieved at low temperature, elevated pressure, and long contact time, while yield and selectivity to acrylic acid are most favorable at high temperature, low pressure, and short contact time. Post-reaction Fourier transform infrared spectroscopic analyses of the catalyst indicate that sodium nitrate as the initial catalyst material is transformed to sodium lactate at the onset of reaction via proton transfer from lactic acid to nitrate. The resultant nitric acid vaporizes as it is formed, leaving sodium lactate as the sole sodium-bearing species on the catalyst during reaction.

INTRODUCTION

The production capacity for lactic acid (2-hydroxypropanoic acid) from biomass sources has increased greatly in the U.S. during the past few years (1, 2), driven primarily by the potential for producing biodegradable polymers. This growing availability of lactic acid, coupled with its reactive nature (containing both a hydroxyl and a carboxyl group), has led us to examine it as a feedstock for biomass and agriculturally based chemical production.

Primary lactic acid conversion pathways are shown in Fig. 1. Dehydration to acrylic acid and cracking to acetaldehyde have been known for many years; the former has been examined as a possible conversion route to acrylate polymers and plastics formation (3–5).We recently discovered the formation of 2,3-pentanedione from lactic acid over supported phosphate catalysts in our laboratory (6), and have examined the activity of a number of different catalyst and support species for 2,3-pentanedione formation (7). The diketone is proposed to form via a Claisen condensation of two lactate moieties followed by decarboxylation and dehydration steps.

We have also examined the species present on the surface of sodium phosphate catalysts via ^{31}P-MAS nuclear magnetic resonance (NMR) and post-reaction Fourier transform infrared (FTIR) spectroscopies (8). These analyses indicate that sodium lactate, formed via proton transfer from lactic acid to phosphate, is a predominant species along with phosphates on the support surface during reaction. We propose that both lactate formation and lactic acid conversion are facilitated by the presence of a liquid phase on the support surface (8).

In this paper, the reaction of lactic acid to produce 2,3-pentanedione and acrylic acid is investigated in detail using sodium nitrate on silica as the initial catalyst material. We have previously used sodium nitrate for 2,3-pentanedione formation from lactic acid (7); nitrate has potential processing advantages as a low-cost, environmentally benign material. We present here optimized operating conditions for the formation of 2,3-pentanedione and acrylic acid over sodium nitrate, examine the transformation of sodium nitrate using previously established post-reaction FTIR analytical techniques, and provide initial catalyst stability and coke deposition data for the system. A systematic experimental design is used to arrive at optimum conditions for conversion to desired products.

METHODS

Materials. The feed used in all experiments is an aqueous solution of 34 wt% L-(-)-lactic acid (Purac, Inc.). This concentration was chosen, based on previous studies, because it is high enough to facilitate significant conversion without leading to plugging of the reactor inlet tube and excessive catalyst coking. High-purity helium (AGA, 99.99%) is used as a diluent and to aid in the vaporization of lactic acid.

The catalyst used in all experiments is sodium nitrate (Aldrich) supported on 80–100 mesh Spherosil XOC-005

[1] To whom all correspondence should be addressed at Department of Chemical Engineering, A202 Engineering Building, Michigan State University, East Lansing, Michigan 48824. E-mail: millerd@che.msu.edu.

0021-9517/97 $25.00

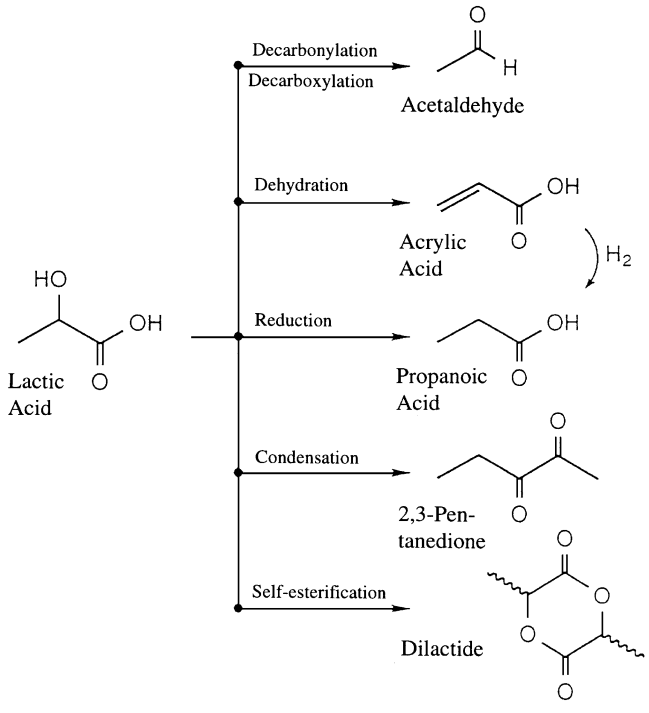

FIG. 1. Lactic acid conversion pathways.

porous silica (Anspec, Inc.; N_2 BET surface area 14 m^2/g). The catalyst was prepared at a loading of 1.0 mmol $NaNO_3$/g support by wet impregnation and drying overnight at 100°C. One batch of catalyst was used for all optimization experiments; 2.0 ± 0.1 g of catalyst was loaded in the reactor in a given experiment.

Reaction system. The reaction system and product analysis techniques used in this study are the same as those described in our earlier studies (6, 7). All reactions are carried out in a vertical, down-flow, fixed-bed integral reactor equipped with a quartz liner. In a typical experiment, fresh catalyst was loaded into the reactor and heated under helium to the initial reaction temperature. The catalyst was then conditioned by exposing it to an elevated flow rate (0.5 ml/min) of lactic acid feed solution for about 15 min (without this it took several hours to reach steady state). The desired feed flow rate for the experiment was then established (0.05–0.5 ml/min) and steady state product collection was begun. Each catalyst was typically tested under three to five sets of reaction conditions before the reactor was shut down, cleaned, and reloaded with fresh catalyst. At a given set of conditions, condensible products and noncondensible products were collected and analyzed separately by gas chromatography. Results of the analyses were entered into a spreadsheet to calculate product yields, selectivities, feed conversion, and an overall carbon balance for the experiment. Product yield is reported as percentage of the theoretical yield based on lactic acid fed to the reactor. The experimental conditions under which reactions were carried out are summarized in Table 1.

Optimization methods. Optimum operating conditions for formation of acrylic acid and 2,3-pentanedione are determined by a two-level, three-parameter factorial design designated as a "Box–Benkhen" design (9). The Box–Benkhen design provides an efficient method for determining product yields over a range of defined reaction conditions (i.e., independent variables) through a limited number of experiments. Implementation of the design involves defining "boundary values" (i.e., minima and maxima) for all reaction parameters, conducting experimental runs at conditions defined by the design, and fitting the resulting product yields to quadratic model equations describing their dependence on reaction conditions.

In this study, three reaction conditions were chosen as independent variables: temperature, contact time, and pressure (x_1, x_2, x_3). The range of these parameters over which experiments were conducted can be thought of as occupying a cube, with the center (0, 0, 0) describing the base set of conditions. Following the Box–Benkhen design, one experiment was conducted at each set of conditions denoted by the midpoints of the twelve cube edges, and four experiments were conducted at conditions corresponding to the center point. These experiments were conducted in random order to avoid any systematic bias in the results. After every three experiments, the reactor was shut down, cleaned, and loaded with fresh catalyst in order to minimize the effects of coke buildup or catalyst deactivation on the results. Additional experiments were also conducted to verify the reliability of the results obtained and extend the study beyond the limits of the experimental design.

In order to identify trends in product yields and optimum reaction conditions, the experimental yield (Y) of acrylic acid and of 2,3-pentanedione were fit to a quadratic model of the form

$$Y = b_0 + b_1x_1 + b_2x_2 + b_3x_3 + b_{12}x_1x_2 + b_{13}x_1x_3 + b_{23}x_2x_3 + b_{11}x_1^2 + b_{22}x_2^2 + b_{33}x_3^2, \quad [1]$$

TABLE 1

Reaction Conditions

Parameter	Range	Box–Benkhen design values		
		−1	0	1
Temperature (°C)	265–370	280	315	350
Pressure (MPa)	0.2–1.0	0.2	0.6	1.0
Contact time (s)	0.3–5.0	0.5	2.2	4.0
Feed composition (mole fraction)		Lactic acid: 0.08 Water: 0.77 Helium: 0.15		
Catalyst mass (g)		2.0 ± 0.1		

where x_1, x_2, and x_3 are again the three independent variables temperature, contact time, and pressure. The coefficients (b_i, b_{ij}) in the model equation were determined by regression analysis using the Linest function in Microsoft Excel 5.0. Contour plots were then produced from Eq. [1] as a function of process conditions to illustrate trends and identify optimum conditions for each of the two desired products.

FTIR spectroscopic analyses. Post-reaction Fourier transform infrared (FTIR) spectroscopy was used to investigate the nature of stable species present on the catalyst and to gain insight into the role of the nitrate catalyst and the mechanism of product formation. These studies were performed using equipment and methods similar to those previously described in (8). Sodium nitrate solution (100 μl, either 5 mmol/liter or 50 mmol/liter) was deposited on both sides of an IR-transparent silicon disk using a micropipet. Water was then removed at ambient temperature under vacuum in a desiccator, leaving a thin layer of $NaNO_3$ on the disk as a model catalyst-support system. The loaded disk was then placed in the IR sample preparation apparatus (8) and exposed to lactic acid vapors for (in most cases) 10 min at a specified temperature. Following exposure to lactic acid, the disk was transferred immediately to a sample holder and placed in a Nicolet IR/42 spectrophotometer wherein the transmission FTIR spectrum was obtained. Subtraction of background and silicon disk spectra gives a spectrum representative of the material on the catalyst surface following reaction at the specified temperature. The entire procedure, starting with the clean silicon disk, was repeated for each temperature studied. This technique facilitates rapid and reliable collection of post-reaction IR spectra; the method gives essentially the same spectra as those taken by diffuse reflectance IR spectroscopy of actual supported catalysts (8) and thus is a valid analytical tool.

RESULTS

Optimization of reaction conditions. Complete results of experiments conducted within the Box–Benkhen design are given in Table 2 in the order they were carried out, with each number (e.g., 18) signifying a particular charge of catalyst to the reactor. Contour plots of 2,3-pentanedione and acrylic acid yields versus temperature and contact time at each pressure studied were generated following regression analysis of the results; representative plots are presented in Fig. 2 for 2,3-pentanedione at 0.6 MPa pressure and in Fig. 3 for acrylic acid at 0.2 MPa. The contour surfaces are generally in the shape of saddles; the highest 2,3-pentanedione yield predicted within the experimental design matrix is 18% at 280°C, 0.6 MPa, and 4 s contact time, and the highest acrylic acid yield predicted is 18% at 350°C, 0.2 MPa, and 0.5 s contact time. Plots at other pressures are qualitatively similar but yields are lower. The regression coefficients (r^2)

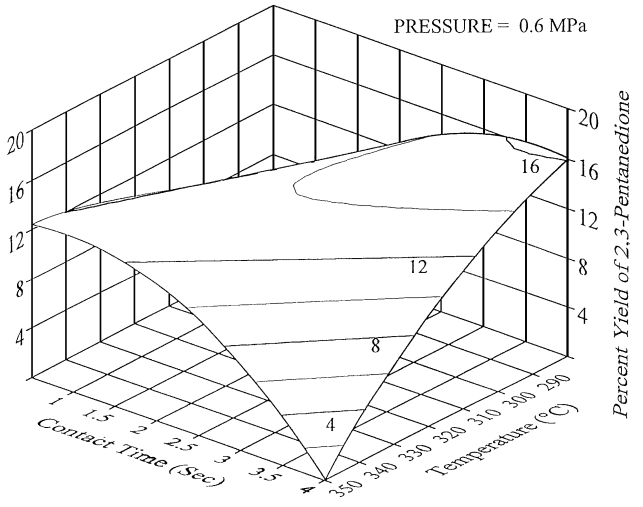

FIG. 2. Contour plot of 2,3-pentanedione yield from regression analysis of experimental data at 0.6 MPa.

for the fits of Eq. (1) to acrylic acid and 2,3-pentanedione yields are 0.81 and 0.83, respectively; the confidence level of the fit, determined by a standard *F*-test (10), is 90% for 2,3-pentanedione and 98% for acrylic acid.

Because maximum product yields were predicted to occur at conditions along the edge of the design matrix, additional experiments were conducted outside the experimental design range to determine if the above results represented true optima. Results of these experiments are given in Table 3 and are described below. Table 3 also includes results of repeated experiments used to verify product yields.

Yield of 2,3-pentanedione drops as temperature is decreased from 280 to 265°C (Exp. 28b) and as pressure

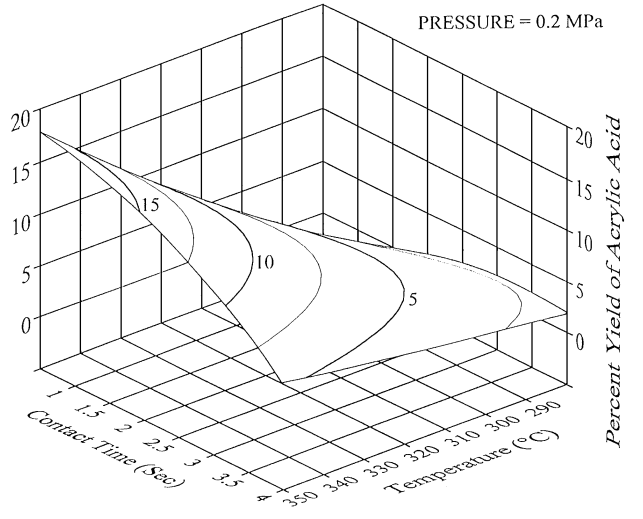

FIG. 3. Contour plot of acrylic acid yield from regression analysis of experimental data at 0.2 MPa.

TABLE 2

Product Yields from Optimization Study[a]

Experiment	18a	18b	18c	19a	19b	19c	20a	20b	20c	21a	21c	22a	22b	22c	23a	23b
Coordinates	(0, 0, 0)	(−1, −1, 0)	(1, 0, −1)	(0, −1, 1)	(−1, 0, −1)	(−1, 1, 0)	(0, −1, −1)	(0, 0, 0)	(1, 1, 0)	(−1, 0, 1)	(0, 1, −1)	(0, 1, 1)	(1, 0, 1)	(0, 0, 0)	(1, −1, 0)	(0, 0, 0)
Temperature (°C)	315	280	350	315	280	280	315	315	350	280	315	315	350	315	350	315
Contact time (s)	2.2	0.5	2.2	0.5	2.2	4.0	0.5	2.2	4.0	2.2	4.0	4.0	2.2	2.2	0.5	2.2
Pressure (MPa)	0.6	0.6	0.2	1.0	0.2	0.6	0.2	0.6	0.6	1.0	0.2	1.0	1.0	0.6	0.6	0.6
Acrylic acid	7.8	0.6	16.7	3.4	3.1	6.6	2.9	12.3	2.2	3.9	2.2	6.9	2.6	9.2	13.5	12.2
2,3-Pentanedione	14	1.6	9.1	8.1	6.1	17.7	3.5	13.2	1.4	10.4	1.8	5.4	1.5	7.4	10.7	15.4
Acetaldehyde	12.5	0.6	7.8	3.1	2.3	6.9	0.8	9.4	10.3	7.0	9.6	13.4	12.6	13.4	6.4	8.8
Propanoic acid	1.6	0.3	3.1	0	1.3	2.8	0.7	2.4	14.4	1.8	12.1	8.0	11.7	6.0	1.2	2.2
Hydroxyacetone	3.1	0	3.5	0.9	2.0	2.7	1.0	6.8	2.7	0.7	5.0	4.2	3.0	5.6	4.5	5.7
Other	6.2	7.2	4.0	1.8	2.3	4.3	3.1	4.2	11.9	3.7	8.0	11.4	12.6	5.9	2.6	4.0
CO	9.1	0.9	4.9	3.7	1.0	3.7	1.2	5.0	6.4	6.4	6.2	3.7	10.0	7.5	3.7	3.8
CO_2	36.7	1.8	16.9	7.6	6.1	15.1	5.0	31.2	24.1	9.4	28.4	18.6	38.8	21.9	20.5	24.9
Lactic conversion	88	15	98	25	63	28	44	85	91	31	90	87	89	92	78	86
Carbon recovery (%)	66	95	50	93	56	113	70	69	56	97	56	63	65	59	65	66

[a] Experiment 21b discounted because of improperly set feed composition.

TABLE 3

Product Yields from Repeated and Extended Experiments[a]

Experiment	23c	24a	24b	26a	26b	26c	27a	27b	27c	27d	28a	28b	28c
Coordinates	(0, −1, −1)	(−1, 1, 0)	(−1, 1, 0.5)	(1.6, −0.2, −0.5)	(−1.4, 0.5, 0)	(−1.4, 0.5, 0.5)	(1.6, −1.2, −0.5)	(1.6, −1.2, −0.5)	(−1.4, 1.5, 0)	(−1.4, 1.5, 0.5)	(1.6, −1, 0.5)	(−1.4, 1, 0)	(−1.4, 1, 0.5)
Temperature (°C)	315	280	280	370	265	265	370	370	265	265	370	265	265
Contact time (s)	0.5	4.0	4.0	1.8	3.1	3.1	0.3	0.3	5.0	5.0	0.5	4.0	4.0
Pressure (MPa)	0.2	0.6	0.8	0.4	0.6	0.8	0.4	0.4	0.6	0.8	0.4	0.6	0.8
Acrylic acid	4.3	5.8	5.8	10.1	2.4	2.3	25.4	19.8	3.6	3.5	26.4	3.1	2.6
2,3-Pentanedione	4.2	20.2	15.3	13.1	7.1	6.5	10.3	7.9	10.4	10.9	12.3	8.0	8.5
Acetaldehyde	3.0	6.1	5.8	22.9	2.9	3.7	9.0	3.7	2.7	4.1	7.4	2.0	5.2
Propanoic acid	1.6	1.9	2.0	13.1	1.3	1.3	4.5	2.4	1.1	1.3	2.6	1.3	1.6
Hydroxyacetone	1.8	1.7	2.1	4.7	0	0	5.0	3.7	0.8	0.8	7.3	0	0.8
Other	2.2	3.7	3.5	9.7	2.4	2.7	3.8	3.4	2.7	2.4	4.9	2.3	3.0
CO	1.1	3.1	1.6	14.9	2.4	2.0	4.8	3.4	1.8	2.2	7.0	2.3	2.7
CO_2	5.3	15.0	8.9	41.6	6.2	4.9	18.4	10.2	9.3	7.3	29.2	7.0	5.9
Lactic conversion	58	52	56	92.0	51	19	92	72	48	63	90	23	33
Carbon recovery (%)	59	87	77	83	66	98	69	70	74	60	79	94	88

[a] Experiment 24c not included because of excessive product loss.

is increased from 0.6 to 0.8 MPa (Exps. 24b, 28c). Increasing contact time from 4 to 5 s at 265°C enhances 2,3-pentanedione yield (Exp. 27c, 27d); unfortunately, we were unable to lengthen contact time beyond 5 s at 265°C in our reactor system as a consequence of bed height and minimum liquid feed rate restrictions. We thus believe 280°C and 0.6 MPa to be optimal conditions, but higher 2,3-pentanedione yields may be achievable at residence times longer than 4–5 s at 280°C.

For acrylic acid formation, increasing temperature to 370°C significantly increases acrylic acid yield at short residence times (Exps. 27a, 27b, 28a); longer residence times at 370°C (Exp. 26a) lead to a decline in acrylic acid yield as a result of an apparent secondary reaction to propanoic acid. We did not examine temperatures above 370°C, because we cannot achieve residence times of less than 0.3 s in our reactor and we expect that secondary reactions will reduce acrylic acid yields at 0.3 s residence time and temperatures above 370°C. Optimum conditions for acrylic acid formation, based on these additional experiments, are 370°C, 0.3–0.5 s contact time, and low pressure (0.1–0.4 Mpa). It is possible, however, that other combinations of temperature and short residence time may lead to higher acrylic acid yields than those achieved here.

The data in Table 3 were combined with those in Table 2 and a second regression analysis was performed to develop contour plots based on all experiments performed. The contour plots obtained were essentially the same as those resulting from regression of the formal Box–Benkhen design only (Figs. 2 and 3) and are thus not reported.

Secondary reactions of acrylic acid and 2,3-pentanedione. To further investigate secondary reaction pathways leading to the observed maxima in acrylic acid and 2,3-pentanedione yields with contact time, we conducted a series of experiments at 0.6 MPa using acrylic acid and 2,3-pentanedione as feed materials.

Over fresh nitrate catalyst or over catalyst previously used for lactic acid conversion, no significant reaction of a 5 wt% solution of 2,3-pentanedione, either alone or in combination with similar quantities of acetaldehyde or acrylic acid, was observed over the range 280–350°C and contact times up to 5 sec. When co-fed with lactic acid over the used catalyst at 350°C and 5 s contact time, however, less 2,3-pentanedione exited the reactor than was expected as the sum of the quantity formed via lactic acid conversion plus the quantity (5 wt%) added to the feed. We thus conclude that secondary reaction of 2,3-pentanedione does take place in the presence of lactic acid and at high temperatures.

For acrylic acid, a feed of 17 wt% acid in water initially pumped into the reactor led to coking and eventual plugging of the catalyst bed, indicating that acrylic acid decomposes or polymerizes over the catalyst. When the feed concentration was reduced to 4 wt%, which corresponds to an acrylic acid yield of about 14% of theoretical, very little coking of the catalyst or conversion of acrylic acid, either fed alone or in combination with lactic acid, acetaldehyde, or 2,3-pentanedione, took place over the range 280–350°C and contact times to 5 sec. We thus conclude that secondary reaction of acrylic acid is important only at high acrylic acid formation rates and product concentrations, and may be a significant source of coking at these conditions.

Application of kinetic model. In our previous work (6), we developed a simple kinetic model and calculated rate constants for lactic acid conversion in our integral fixed-bed catalytic reactor. The molar balances for the three major species are written as follows, with concentrations of lactic acid, 2,3-pentanedione, and acrylic acid denoted by C_L, C_P, and C_A respectively, and residence time by τ.

$$\frac{dC_L}{d\tau} = -k_1 C_L - 2k_2 C_L^2 - k_3 C_L \quad [2]$$

$$\frac{dC_P}{d\tau} = k_2 C_L^2 - k_5 C_P \quad [3]$$

$$\frac{dC_A}{d\tau} = k_3 C_L - k_4 C_A \quad [4]$$

The balances include a first-order rate expression for formation of acrylic acid, a first-order rate expression for formation of acetaldehyde plus propanoic acid, hydroxyacetone, and "other" products together, and a second-order rate expression for formation of 2,3-pentanedione. The model also includes first-order decomposition pathways for acrylic acid and 2,3-pentanedione. The model was applied to the results of this study (Tables 2 and 3) by simultaneously varying the preexponential factors ($k_{i,o}$) and activation energies (E_i) of rate constants k_1 through k_5 (in the standard Arrhenius form) for the five reaction steps using Excel 5.0 to minimize the sum-of-squares residuals of species' exit concentrations and lactic acid conversion for all experimental runs. The resulting rate constants for each reaction are given in Table 4. Turnover frequencies (TOF) for each reaction step are also given in Table 4 at the centerpoint conditions (0, 0, 0) and at 50% lactic acid conversion in the reactor. The TOF calculation is based on a catalyst loading of 1.0 mmol/g; we have previously shown that mass transport limitations do not affect reaction rates at these reaction conditions (6).

Extended reaction. Stability of the nitrate catalyst for acrylic acid and 2,3-pentanedione formation was tested by conducting an extended run for a 24 hr period at 350°C, 0.6 Mpa, and 1.0 s contact time. These conditions were chosen to give reasonably high yields of both acrylic acid and 2,3-pentanedione. Average yield for acrylic acid was 24%, for 2,3-pentanedione it was 14%, for acetaldehyde 9%, and for propanoic acid 4%; the average lactic acid conversion was about 88%. Product yields and conversion were essentially constant over the 24 hr experiment, indicating

TABLE 4

Rate Constants from Kinetic Model

Reaction	Reaction order	Preexponential factor ($k_{i,o}$)	Activation energy (kJ/mol)	TOF[a] (s^{-1})
Lactic acid → Acetaldehyde + Others	1	9.7×10^9 s^{-1}	115	5.7×10^{-3}
Lactic acid → 2,3-Pentanedione	2	6.5×10^{10} liter mol^{-1} s^{-1}	110	1.1×10^{-3}
Lactic acid → Acrylic Acid	1	1.9×10^{11} s^{-1}	137	1.2×10^{-3}
Acrylic acid → Products	1	7.2×10^{10} s^{-1}	132	1.9×10^{-4}
2,3-Pentanedione → Products	1	2.0×10^{11} s^{-1}	138	1.1×10^{-4}

[a] Turnover frequency determined at centerpoint conditions (315°C, 0.6 MPa) at 50% lactic acid conversion in reactor.

that the catalyst is stable and remains active at these conditions.

Coke deposition. Weight gain of the catalyst and reactor tube was measured upon reactor disassembly at the end of each experiment. Coke deposits were consistently observed on the reactor walls above the catalyst, in the greatest amount at the top of the catalyst bed, and to a lesser degree through the length of the bed. We attribute this coke deposition to feed lactic acid and its oligomers, both of which have low volatility and are thus prone to decomposition prior to vaporization.

The quantity of coke deposited and its contribution to the overall carbon balance is reported in Table 5. For the purpose of conducting the carbon balance, we assume the coke deposited contains 50% carbon by weight. (This is reasonable and conservative; polylactic acid contains 50% carbon by weight and further decomposition of the polymer would lead to a higher carbon content.) Carbon recovery in products exiting the reactor was measured by averaging each individual run weighted to the quantity of feed input during that run. It is seen that solids deposition in most experiments accounts for most of the carbon absent from the recovered products. It is interesting that the quantity of coke deposited during the extended (24 hr) run is only slightly higher than the average quantity deposited during the typical experiment of 4–5 hr duration, suggesting that coke deposition slows over extended reaction times.

TABLE 5

Summary of Carbon Deposition and Carbon Recovery

Experiment	Carbon deposited[a] over experiment (g)	Average carbon recovery[b] in products over experiment (percent carbon fed)	Carbon deposited[c] over experiment (percent carbon fed)
18	1.54	77	16
20	1.05	67	15
21	1.98	77	33
22	1.76	62	25
26	1.87	82	26
27	0.84	69	7
28	1.30	85	14
Extended run	1.81	86	3

[a] Absolute quantity of solids deposited; catalyst weight 2.0 ± 0.1 g in each experiment.

[b] Based on product recovery from each run weighted to total feed volume during run.

[c] Solids deposited on catalyst and reactor walls assumed to contain 50% carbon by weight.

FTIR analyses. Results of post-reaction transmission FTIR analyses are given in Figs. 4–7: only the portion of the IR spectrum from 700 to 2000 cm^{-1} is reported, as the most important spectral information is contained within this region. To verify thermal stability of the nitrate catalyst over the temperature range of interest, FTIR spectra of sodium nitrate deposited on the silicon disk (100 μl of 5 mmol/liter solution) and then exposed only to water vapor at different temperatures were collected and are reported in Fig. 4. Key features of the sodium nitrate spectrum include sharp peaks at 836 and 1788 cm^{-1}, a broad, strong peak centered at 1355 cm^{-1}, and a weaker band at 2430 cm^{-1} (not shown). These absorption bands are in agreement with those reported in the literature for sodium nitrate (11–14). Figure 4 clearly shows that sodium nitrate is thermally stable over the range of temperatures studied.

Spectra for sodium nitrate exposed to lactic acid vapors at different temperatures were collected at two different nitrate loadings on the disk: 100 μl of 5 mmol/liter solution (Fig. 5) and 100 μl of 50 mmol/liter solution (Fig. 6) Figure 5 shows that no nitrate is observable on the disk at low loadings at any of the temperatures studied. Sodium lactate is observed at all temperatures, as evidenced by a strong peak at 1599 cm^{-1} (C=O stretch) and several weaker bands at 1050–1424 cm^{-1} (15, 16). Some lactic acid is also present, as seen by its strong C=O stretching frequency at 1730 cm^{-1} (15, 16). Reference spectra for lactate species are not given here, but have been collected by us (8) and agree with the literature spectra (15, 16).

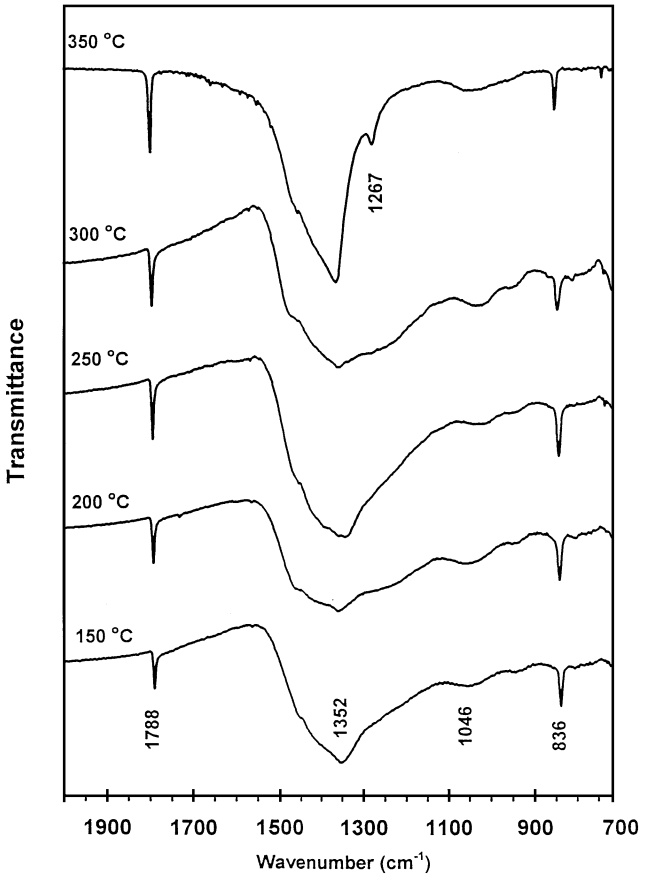

FIG. 4. FTIR spectra of species present on sodium nitrate-loaded silicon disk (100 μl of 0.005 *M* $NaNO_3$ solution) following exposure to water vapor at different temperatures.

Figure 6 gives IR spectra for the silicon disk carrying 10 times the quantity of nitrate as used for spectra reported in Fig. 5. In Fig. 6, sodium nitrate is seen to remain on the disk at temperatures up to 300°C following a 10-min exposure to lactic acid. Above 300°C, nitrate disappears and sodium lactate is observed in large quantities with little lactic acid present. These results with more nitrate on the support disk suggest that the consumption of nitrate is kinetically limited on the disk surface. Exposure of the disk at 300°C for longer time periods shows that the nitrate peak disappears (Fig. 7), further indication of the kinetic limitations of proton transfer.

DISCUSSION

The kinetic model (Table 4) predicts the favorability of acrylic acid formation at high temperatures, short contact times, and low pressures, and the favorability of 2,3-pentanedione at low temperature, long contact times, and elevated pressure. The activation energy calculated for acrylic acid formation is the same as the calculated previously for phosphate salts (6); the activation energies for 2,3-pentanedione and acetaldehyde plus other species formation are somewhat (~30 kJ/mol) higher than those calculated for phosphates. Turnover frequencies calculated here are based on the assumption that all catalyst is participating in the reaction, even though sufficient sodium lactate is present to form 20–30 monolayers on the silica surface. The IR results clearly show that all nitrate initially present is converted to lactate, and our postulate that the catalyst is present as a molten phase on the catalyst surface (see below) is consistent with all catalyst being taken as active. The magnitude of the turnover frequencies are low; TOF for product decomposition pathways are of the order of 15–20% of the corresponding product formation pathways at the conditions specified.

The kinetic model predicts product yields and conversions reasonably well over the entire range of reaction conditions, but the experimental results at 1.0 MPa do not match model predictions as well as those at lower pressures. First, the experimentally observed yields of 2,3-pentanedione increase significantly from 0.2 to 0.6 MPa total pressure, but little further increase is observed as pressure is raised to 1.0 MPa. The kinetic model predicts that 2,3-pentanedione formation should increase with total

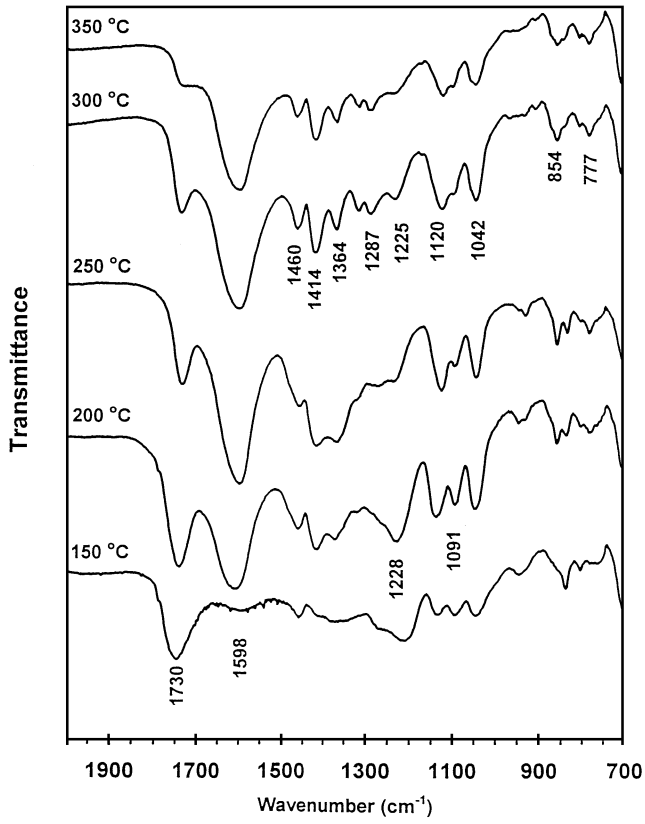

FIG. 5. FTIR spectra of species present on sodium nitrate-loaded silicon disk (100 μl of 0.005 *M* $NaNO_3$ solution) following exposure to lactic acid at different temperatures.

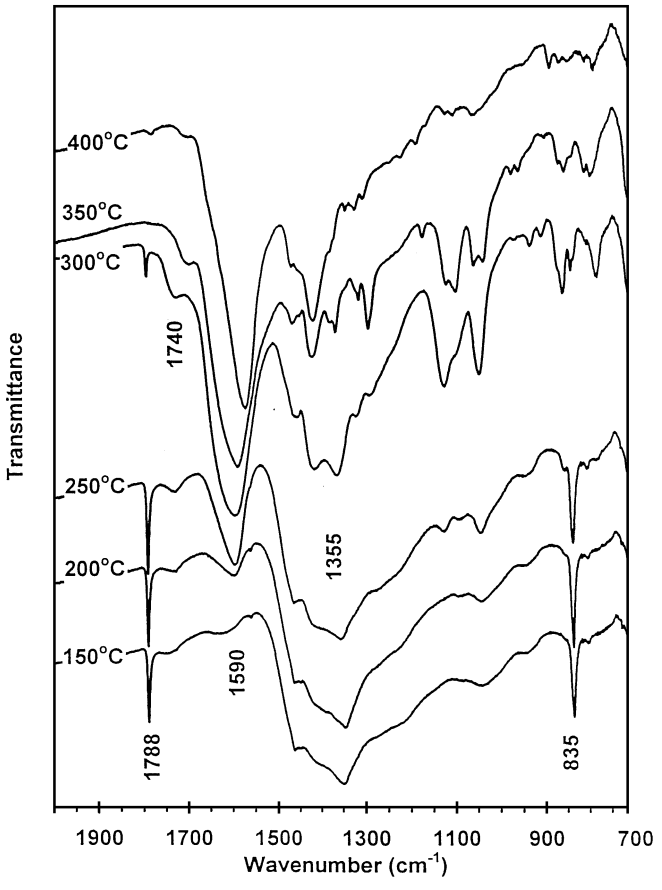

FIG. 6. FTIR spectra of species present on sodium nitrate-loaded silicon disk (100 μl of 0.050 *M* $NaNO_3$ solution) following exposure to lactic acid at different temperatures.

pressure, as expected for a second-order reaction, although the predicted increase is small at high temperatures and long contact times because of competing reaction pathways and depletion of reactant.

Second, trends in acetaldehyde yield deviate from trends predicted by the model in several sets of experiments (19b, 21a and 19a, 20a) where only total pressure is changed from 0.2 to 1.0 MPa. In these experiments the yield of acrylic acid remains essentially constant (as expected for a first-order dominated reaction), but the yield of acetaldehyde (also formed via a first-order pathway) increases significantly and corresponding CO formation increases as well. It thus appears that lactic acid decomposes to acetaldehyde via a pathway not present in the kinetic model.

We attribute these differences in experimental and predicted yields at higher pressures to the increased difficulty in vaporizing lactic acid as it enters the reactor at high pressure. Lactic acid vaporizes completely only at reduced pressure and is known to dimerize (and thus become essentially nonvolatile) along with vaporizing during heating (17, 18). Further, in a previous study (19) we have observed acetaldehyde formation in condensed-phase pyrolysis of lactic acid; thus additional acetaldehyde is formed at higher pressures by decomposition of unvaporized lactic acid which has entered the reactor. For 2,3-pentanedione, yield does not increase as pressure is increased from 0.6 to 1.0 MPa because a greater fraction of the entering lactic acid decomposes prior to exposure to the catalyst at 1.0 MPa and is thus unavailable for diketone formation.

Lactic acid decomposition prior to vaporization is also responsible for most of the coke deposited during reaction, as evidenced by the majority of coke on the reactor walls above and directly on the top of the catalyst bed. As seen in Table 5, carbon balances are close for the most part when coking is taken into account (the two right-hand columns add to 100% at closure), especially recognizing that lactic acid analysis by gas chromatography is only accurate to within ±14% (6). Even for those experiments where carbon balance closure is still incomplete, we have shown previously that product distributions depend only slightly on carbon recoveries (6, 7) and thus have confidence that product yields reported are a true representation of the reaction system. It is unfortunate that the contribution of coking to the carbon balance and the overall reaction system cannot be treated any further than was reported in Table 5: because

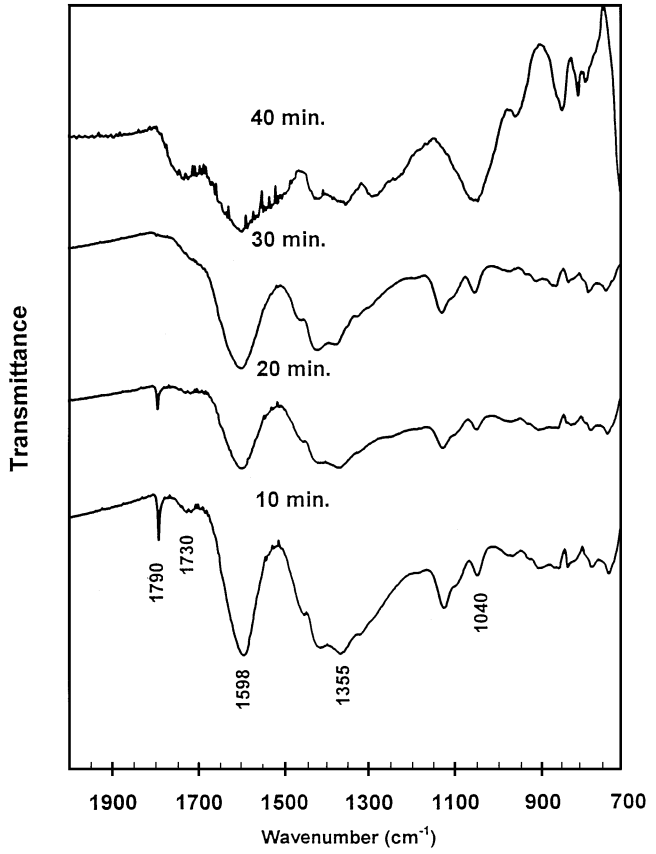

FIG. 7. FTIR spectra of species present on sodium nitrate-loaded silicon disk (100 μl of 0.050 *M* $NaNO_3$ solution) following exposure to lactic acid at 300°C for different lengths of time.

coke deposition takes place for the most part above the catalyst bed, there is no way to incorporate it as a reaction into the ideal, plug-flow reactor model used to generate the kinetic constants. The same holds true for acetaldehyde formed via condensed lactic acid decomposition at higher pressures.

Finally, the extended run shows that the catalyst is stable for formation of 2,3-pentanedione and acrylic acid even upon substantial coke deposition over the course of the experiment. Apparently there is not enough coke deposited in the catalyst bed to substantially deactivate the sodium lactate over the time scale of the experiment conducted. It may be that the reactions occur on the coke as well as on the silica support, but based on earlier studies with carbon supports (7), where we observed little 2,3-pentanedione or acrylic acid formation, we do not believe that this is the case.

FTIR experiments. Post-reaction FTIR transmission spectroscopic analyses of model catalyst surfaces show that sodium nitrate is consumed upon exposure to lactic acid. The absence of nitrate and presence of sodium lactate at high temperatures indicates that lactic acid transfers a proton to sodium nitrate to form nitric acid and sodium lactate:

$$NaNO_3 + HC_3H_5O_3 \rightleftarrows HNO_3 + NaC_3H_5O_3 \quad [5]$$

Nitric acid has a normal boiling point of 80°C; it also forms a binary azeotrope with water that boils at 120°C (at atmospheric pressure) and thus vaporizes as it is formed on the support. The proton transfer reaction can therefore proceed to completion, despite the unfavorable pK_a difference between nitric acid (p$K_a = -1.4$) and lactic acid (p$K_a = 3.1$). The dominant, stable species on the catalyst surface is sodium lactate, which must play a primary role in 2,3-pentanedione and acrylic acid formation.

The proton transfer in Eq. [5] agrees with our findings over phosphate salts (8), in which lactic acid transferred a proton to trisodium phosphate to form sodium lactate and disodium phosphate, which subsequently condensed to tetrasodium pyrophosphate. Based on the nitrate results presented here, in which higher yields of 2,3-pentanedione and acrylic acid are achieved than with the phosphate salt, and that only sodium lactate is observable, we conclude that the phosphate played no role of consequence in the formation of desirable products. In fact, silica-supported sodium lactate itself is as effective a catalyst as sodium nitrate for lactic acid conversion to 2,3-pentanedione. Thus, the alkali salt catalysts active for lactic acid conversions only serve as sources of alkali metal cations which form lactate salts upon exposure to lactic acid. The conversion of lactic acid to acrylic acid and 2,3-pentanedione takes place upon interaction of lactic acid with sodium lactate.

The accessibility of the proton transfer reaction (despite the unfavorable pK_a difference between nitric and lactic acid) is confirmed by an experiment in which the weaker propanoic acid (p$K_a = 4.9$) was passed over a sodium nitrate-loaded silicon disk. The FTIR spectra as a function of temperature are given in Fig. 8; formation of sodium propanoate along with the disappearance of nitrate is clearly seen at 300°C and above.

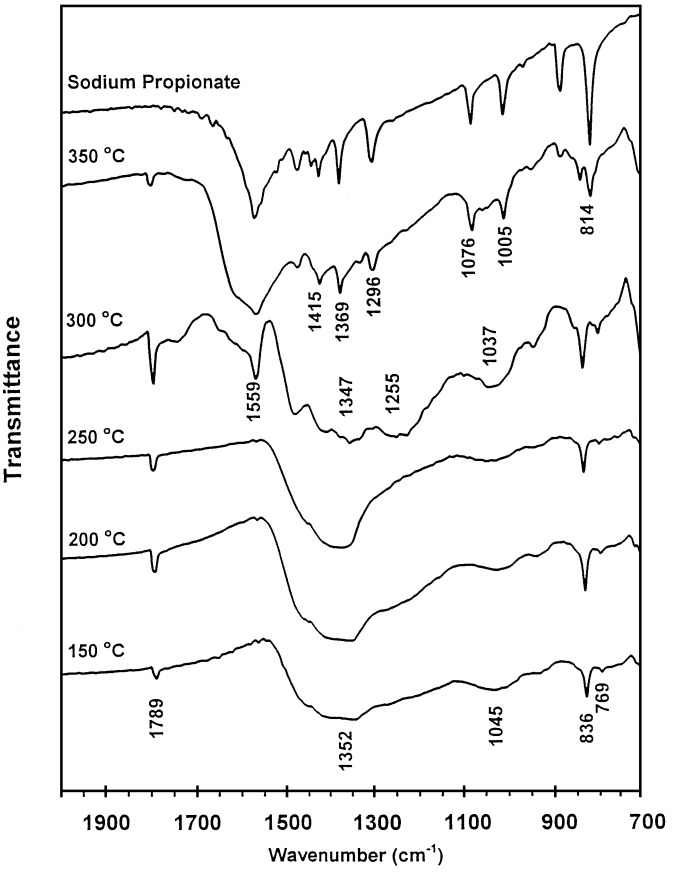

FIG. 8. FTIR spectra of species present on sodium nitrate-loaded silicon disk (100 μl of 0.005 *M* $NaNO_3$ solution) following exposure to propanoic acid at different temperatures.

We are continuing investigations of the mechanism of 2,3-pentanedione and acrylic acid formation over alkali metal salt catalysts. We now know that proton transfer to the salt from lactic acid occurs on the support surface; Figs. 4 and 5 show that this transfer is not necessarily rapid and may take substantial exposure time at reaction temperature to reach completion. We postulate the presence of a liquid phase on the support that expedites proton transfer as well as condensation to 2,3-pentanedione and dehydration to acrylic acid.

ACKNOWLEDGMENTS

The support of USDA Grant 93-37500-9585, under the National Research Initiative, is greatly appreciated. Support of the Crop and Food Bioprocessing Center by the State of Michigan Research Excellence Fund is also gratefully acknowledged.

REFERENCES

1. Lipinsky, E. S., and Sinclair, R. G., *Chem. Eng. Prog.* **82**(8), 25 (1986).
2. Keeler, R., *Res. Dev.*, 52 (February 1991).
3. Fisher, C. H., and Filachione, E. M., U.S. Department of Agriculture, Bur. Agr. and Ind. Chem. AIC-279 (1950).
4. Holman, R. E., U.S. Patent 2,859,240 (1958).
5. Sawicki, R. A., U.S. Patent 4,729,978 (1988).
6. Gunter, G. C., Jackson, J. E., and Miller, D. J., *J. Catal.* **148**, 252 (1994).
7. Gunter, G. C., Langford, R. H., Jackson, J. E., and Miller, D. J., *Ind. Eng. Chem. Res.* **34**, 974 (1995).
8. Gunter, G. C., Tam, M. S., Craciun, R., Jackson, J. E., and Miller, D. J., *J. Catal.*, **164**, 207 (1996).
9. Box, G. E. P., Hunter, W. G., and Hunter, W. S., "Statistics for Experimenters: An Introduction to Design, Data Analysis, and Model Building," Wiley, New York, 1978.
10. Dixon, W. J., and Massey, F. J., Jr., "Introduction to Statistical Analysis," McGraw–Hill, New York, 1957.
11. Vratny, F., *Appl. Spectrosc.* **13**(3), 59 (1959).
12. Ferraro, J. R., *J. Molec. Spectrosc.* **4**, 99 (1960).
13. Williamson, K., Li, P., and Devlin, J. P., *J. Chem. Phys.* **48**, 3891 (1968).
14. Nakagawa, I., and Walter, J. L., *J. Chem. Phys.* **51**, 1389 (1969).
15. Cassanas, G., Morssli, M., Fabregue, E., and Bardet, L., *J. Raman Spectrosc.* **22**, 409 (1991).
16. Simons, W. M. (Ed.), "The Infrared Spectra Handbook of Inorganic Compounds," Sadtler Research Laboratories, Philadelphia, PA, 1984.
17. Nielsen, J. I., and Veibel, M., *Acta Polytech. Scand. Chem. Meatall. Ser.* **63** (1967).
18. Mok, W., Antal, M. J., Jr., and Jones, M., *J. Org. Chem.* **54**, 4596 (1989).
19. Gunter, G. C., "Catalytic Upgrading of Lactic Acid over Supported Salt Catalysts," Ph.D. dissertation. Michigan State University, 1994.